Mechanisms of membrane rupture: From cracks to pores

Zicong Zhou and Béla Joós*
Ottawa Carleton Institute of Physics, University of Ottawa Campus, Ottawa, Ontario, Canada K1N 6N5
(Received 9 January 1997)

The rupture kinetics under isotropic tension of solid membranes with central-force interactions are studied as a function of temperature and the range of the interparticle interactions. At zero temperature, rupture occurs homogeneously at the mechanical instability point. At low temperature, rupture is heterogeneous, mainly by the nucleation of a single crack, branching out into several cracks. This is accompanied by a homogeneous expansion, and the critical rupture tension drops very rapidly with increasing temperature. At high temperature, rupture involves the nucleation of dislocation dipoles, merging to form pores, and the critical rupture tension varies almost linearly with temperature. The temperature T_1, separating these two regimes, is higher the shorter the range of interaction, for potentials of equal depth. We find that under isotropic tension, the crack favors the path along the direction with lowest surface energy, in contrast to that observed under uniaxial tension. The identification of the rupture point is facilitated by the fact that the elastic constants, in particular the bulk modulus, usually show precursor effects. Transverse fluctuations can play an important role as evidenced by a one-dimensional model of self-assembled particles in a ring, pressurized by an ideal gas. These fluctuations are dominant at high temperature, where the rupture pressure is only weakly dependent on temperature. [S0163-1829(97)02330-8]

I. INTRODUCTION

Under the application of increasing stress, a membrane will eventually rupture. The rupture of membranes has been extensively studied experimentally especially for biological membranes.[1–6] But the kinetics are not well understood. Previous existing theoretical studies have concentrated usually on the mechanical forces ignoring the effects of temperature.[7,8] Recently, pores, which are a common feature in the rupture of biological membranes, have been the focus of two statistical-mechanics studies.[9,10]

In contrast to bulk materials where the usual conditions are the application of uniaxial tensile stress, a more relevant situation for membranes is isotropic stress. In this paper we show, with molecular-dynamics (MD) simulations, how, with increasing temperature, monolayers with central-force interactions, go from rupture through the formation of cracks to processes dominated by the formation of pores. The kinetics are found to be very sensitive to the range of the interparticle interaction. In brief, crack propagation is prevalent in the system with nearest-neighbor interaction. And the opposite is true for the longest-range force system, with a Lennard-Jones-type (LJ) potential of the form $(r^{-8}-r^{-4})$ whose range is about five atomic spacings. A crack propagation regime is hard to identify in the latter system. The intermediate range LJ monolayer (LJM) shows both regimes.

In this paper we also consider the relationship between rupture and mechanical instability, by studying the variation of the elastic constants with stress. We find that the rupture point is below the mechanical instability point except at zero-temperature where the two points coincide. Precursor effects in the bulk modulus and the internal pressure are observed close to rupture. In the zero temperature study, some simple analytical expressions are obtained for the elastic stiffness coefficients for systems with three kinds of interaction, at zero temperature and under isotropic tension.

Most of the work is on two-dimensional (2D) flat membranes which do not have a third degree of freedom. To examine the effects of out-of-plane fluctuations, we introduce a simple model of self-assembling particles which we use to consider one-dimensional (1D) closed membranes (two-dimensional vesicles). These exhibit two very distinct regimes of rupture. The high-temperature behavior is in particular interesting with the critical rupture pressure having little dependence on temperature.

The paper is organized as follows. We first introduce the model of the 2D flat membranes (Sec. II). Section III discusses, for these systems, mechanical instability criteria, while in Sec. IV the results of the molecular-dynamics simulations are presented. Section V presents the 1D closed membranes, i.e., 2D vesicles. We conclude in Sec. VI with a discussion.

II. THE TWO-DIMENSIONAL MODEL

The model consists of monolayers of particles interacting with central forces. Several potentials are considered.

One of the simplest interactions is the nearest-neighbor piecewise linear force potential (PLFP) which yields a linear restoring force between nearest-neighbor particles. The potential is given by

$$\phi_{\mathrm{PLFP}}(r)=\begin{cases}\frac{1}{2}\kappa(r-d_0)^2-\kappa w^2 & r\leqslant d_0+w,\\ -\frac{1}{2}\kappa(r-d_0-2w)^2 & d_0+w<r\leqslant d_0+2w,\\ 0 & r>d_0+2w,\end{cases} \tag{1}$$

where r is the distance between atoms, d_0 is the equilibrum lattice spacing in the stress-free state, and w is taken to be $0.15d_0$ as in Ref. 11 For this value of w the dislocation core has only one broken bond. Smaller values of w lead to more

broken bonds in the core. There is no strong core repulsion in this potential, and under moderate compressive pressure there are only nearest-neighbor interactions between atoms.

Another simple potential, the LJ potential (LJP) or 6-12 potential is also well known. It is given by

$$\phi_{\mathrm{LJP}}(r)=4\epsilon\left[\left(\frac{\sigma}{r}\right)^{12}-\left(\frac{\sigma}{r}\right)^{6}\right]. \tag{2}$$

The LJP provides a reasonable description of the properties of rare gases, via computer simulations, if the parameters ϵ and σ are chosen appropriately. There is a negative well of depth ϵ at $2^{1/6}\sigma$, responsible for cohesion in condensed phases. And there is a steeply repulsive wall at short distances less than $r\sim\sigma$, due to nonbonded overlap between the electron clouds. The cutoff for the LJP in our simulations was chosen to be $r_c=3.0\sigma$. The LJP is simply viewed here as a model potential with a hard core and a range exceeding nearest neighbor.

The LJP and PLFP have been extensively used although for different purposes. The PLFP has been used mostly in simulations of the plasticity of solids.[11–14] Whereas the LJP was used extensively in attempts to understand the nature of the melting transition in two dimensions (for reviews see Refs. 15–17). More recently the melting behavior of the PLFP was also considered.[18] Due to their simplicity, the PLFP and LJP systems are still the first systems which come to mind when a simple model for structural properties of materials is being sought.[19,20]

In addition to the above two potentials, we have also considered monolayers with a 4-8 potential (4-8P), to explore further the effect of the range of the interaction potential:

$$\phi_{4-8\mathrm{P}}(r)=4\epsilon'\left[\left(\frac{\sigma'}{r}\right)^{8}-\left(\frac{\sigma'}{r}\right)^{4}\right]. \tag{3}$$

The advantages of the 4-8P are that it is easy to compare with the LJP and PLFP and that it has a longer range than either of the other two potentials. The potential has a negative well of depth ϵ' at $2^{1/4}\sigma'$. The cutoff was chosen to be $r_c=3.0^{1.5}\sigma'$.

To facilitate comparisons, the three potentials have been chosen to have the same depth κw^2, and the same minimum ($\sigma=2^{-1/6}d_0$, $\sigma'=2^{-1/4}d_0$). For the PLFP, the depth is set by the value of w which has been taken as $0.15d_0$, consequently, for the LJP and 4-8P, $\epsilon=\epsilon'=0.0225\kappa d_0^2$.

III. MECHANICAL INSTABILITY CRITERIA AND THE CALCULATION OF ELASTIC CONSTANTS

Elasticity theory can make predictions based on stability criteria as to when a membrane should rupture.

A. General form

It has been shown recently,[21,22] that under constant loading, a system is stable if the following tensor $C_{\alpha\beta\sigma\tau}$ is positive definite:

$$C_{\alpha\beta\sigma\tau}\equiv\mathring{C}_{\alpha\beta\sigma\tau}-\frac{1}{2}(\mathring{S}_{\alpha\beta}\delta_{\sigma\tau}+\mathring{S}_{\sigma\tau}\delta_{\alpha\beta}-\mathring{S}_{\alpha\sigma}\delta_{\beta\tau}-\mathring{S}_{\alpha\tau}\delta_{\beta\sigma}-\mathring{S}_{\beta\tau}\delta_{\alpha\sigma}-\mathring{S}_{\beta\sigma}\delta_{\alpha\tau}), \tag{4}$$

where the $\mathring{C}_{\alpha\beta\sigma\tau}$ are second-order elastic constants defined by

$$\mathring{C}_{\alpha\beta\sigma\tau}\equiv\frac{1}{V_0}\left(\frac{\partial^2 W}{\partial\eta_{\alpha\beta}\partial\eta_{\sigma\tau}}\right)_{\eta=0}, \tag{5}$$

with W being the strain energy. W depends on the ensemble used. It refers to the Helmholtz free energy F for the isothermal elastic constants of the canonical ensemble, i.e., the TVN ensemble in computer simulations (T is the temperature, V the volume, and N the number of particles) or to the internal energy E for the adiabatic elastic constants of the microcanonical ensemble. V_0 is the reference value of the volume V, i.e., before deformation, and $\eta_{\alpha\beta}$ the Lagrangian strain tensor.[23–25] The $\mathring{S}_{\alpha\beta}$ are equal to the applied stress, negative for compression. For a system under hydrostatic pressure p, $\mathring{S}_{\alpha\beta}=-p\delta_{\alpha\beta}$, the $C_{\alpha\beta\sigma\tau}$ are equal to elastic stiffness coefficients[21,22] which govern stress-strain relations, and

$$C_{\alpha\beta\sigma\tau}=\frac{1}{V_0}\left(\frac{\partial^2 G}{\partial\eta_{\alpha\beta}\partial\eta_{\sigma\tau}}\right)_{\eta=0}, \tag{6}$$

where G is Gibbs free energy or the enthalpy.

B. Application to 2D system under hydrostatic pressure

For an isotropic 2D system under hydrostatic pressure, there are only two independent $C_{\alpha\beta\sigma\tau}$, which, in condensed notation, are $\lambda\equiv C_{1122}=C_{12}$ and $\mu\equiv C_{1212}=C_{44}$. In the canonical ensemble with central force interactions, they can be calculated from the expressions[22]

$$\begin{aligned}\lambda=&\frac{1}{k_BT\langle A\rangle}\left\{\left\langle\sum_{i<j}\frac{\phi'}{r}(\Delta x)^2\right\rangle\left\langle\sum_{i<j}\frac{\phi'}{r}(\Delta y)^2\right\rangle\right.\\&\left.-\left\langle\sum_{i<j}\frac{\phi'}{r}(\Delta x)^2\sum_{i<j}\frac{\phi'}{r}(\Delta y)^2\right\rangle\right\}+\frac{1}{\langle A\rangle}\\&\times\left\langle\sum_{i<j}\frac{\phi''}{r^2}(\Delta x)^2(\Delta y)^2\right\rangle-\frac{1}{\langle A\rangle}\left\langle\sum_{i<j}\frac{\phi'}{r^3}(\Delta x)^2(\Delta y)^2\right\rangle\\&-\frac{1}{2\langle A\rangle}\left\langle\sum_{i<j}r\phi'\right\rangle+\frac{Nk_BT}{\langle A\rangle}\\=&\mathring{C}_{12}+p,\end{aligned} \tag{7}$$

TABLE I. r_i and $\Sigma x_i^2 y_i^2$ for triangular lattice up to the 11th neighbors (Z is the number of neighbors).

Neighbor	1st	2nd	3rd	4th	5th	6th	7th	8th	9th	10th	11th
Z	6	6	6	12	6	6	12	6	12	12	6
r_i/d	1	$\sqrt{3}$	2	$\sqrt{7}$	3	$\sqrt{12}$	$\sqrt{13}$	4	$\sqrt{19}$	$\sqrt{21}$	5
$\Sigma x_i^2 y_i^2/d^4$	0.75	6.75	12	37.5	60.75	108	253.5	192	805.5	843.75	468.75

$$\mu=\frac{1}{k_BT\langle A\rangle}\left\{\left\langle\sum_{i<j}\frac{\phi'}{r}\Delta x\Delta y\right\rangle^2-\left\langle\left(\sum_{i<j}\frac{\phi'}{r}\Delta x\Delta y\right)^2\right\rangle\right\}+\frac{1}{\langle A\rangle}\left\langle\sum_{i<j}\frac{\phi''}{r^2}(\Delta x)^2(\Delta y)^2\right\rangle-\frac{1}{\langle A\rangle}\times\left\langle\sum_{i<j}\frac{\phi'}{r^3}(\Delta x)^2(\Delta y)^2\right\rangle+\frac{1}{2\langle A\rangle}\left\langle\sum_{i<j}r\phi'\right\rangle=\mathring{C}_{44}-p, \tag{8}$$

$$p=\frac{Nk_BT}{\langle A\rangle}-\frac{1}{2\langle A\rangle}\left\langle\sum_{i<j}r\phi'\right\rangle, \tag{9}$$

where the quantities Δx and Δy represent the x and y coordinates of $(\mathbf{x}_i-\mathbf{x}_j)$, r the modulus of that vector, and A the area of the system. The $\langle\cdots\rangle$ designate configurational averages. The sums are over all pairs of particles. The stability conditions are then[21,22]

$$B=\lambda+\mu>0$$

and

$$\mu>0, \tag{10}$$

where B is the bulk modulus.

In uniform dilation ensembles,[26] including the TpN ensemble, in which the shape of the MD cell is fixed and the variations of the MD cell lengths l_1, l_2, and l_3 satisfy $l_1/l_{0_1}=l_2/l_{0_2}=l_3/l_{0_3}$, it has been shown[27] that Eq. (8) is still valid, but Eq. (7) fails. In the present work we calculated μ using Eq. (8) in both the TVN and TpN ensembles, and found that they agree to within 1%.

In uniform dilation ensembles, one can find B from

$$\frac{k_BT\langle A\rangle}{B}=\langle A^2\rangle-\langle A\rangle\langle A\rangle. \tag{11}$$

However, as we discussed in Ref. 27, the rate of convergence of Eq. (11) is unsatisfactory in simulations. Therefore, we calculated B using Eqs. (7) and (8) in the TVN ensemble.

For a 2D simple Bravais lattice at zero temperature and hydrostatic pressure p, using periodic boundary conditions Eqs. (7)–(9) can be further simplified to

$$\lambda=\lambda_0+p,\quad \mu=\lambda_0-p,$$

$$\lambda_0=\frac{1}{2a}\sum_{r_i\neq 0}\left(\frac{\phi''(r_i)}{r_i^2}-\frac{\phi'(r_i)}{r_i^3}\right)x_i^2y_i^2,$$

$$p=-\frac{1}{4a}\sum_{r_i\neq 0}r_i\phi'(r_i), \tag{12}$$

where a is the area of the unit cell; the origin of the coordinate system is a lattice point and the summation is over the coordinate of all lattice points except the origin. λ_0 is actually equal to the elastic constants $\mathring{C}_{44}$ and $\mathring{C}_{12}$. Without computing the sums, some conclusions can be drawn from these formulas. If $p>0$ (compression), then $\lambda+\mu>2\mu$, and the shear instability will always occur prior to the spinodal instability (in the sense of vanishing bulk modulus, i.e., $B=\lambda+\mu=0$). In contrast, if $p<0$ (expansion), then $\lambda+\mu<2\mu$ and the spinodal instability will always occur prior to the shear instability. The spinodal instability corresponds to rupture. We can expect these conclusions to be also valid at low temperature. In three dimensions $B=(3\lambda+2\mu)/3$, and such a simple argument cannot be made.

r_i and $\Sigma x_i^2 y_i^2$ up to the 11th neighbors for a triangular lattice can be found in Table I. For the piecewise linear force monolayer (PLFM), using Eq. (12) and noting that for a perfect triangular system with $d\geq 0.75d_0$ we only need to consider six nearest neighbors, we obtain

$$\lambda=\begin{cases}\frac{\sqrt{3}}{4}(5\rho^{1/2}-4)\kappa & 0.75d_0\leq d\leq 1.15d_0,\\ \frac{\sqrt{3}}{4}(4-6.5\rho^{1/2})\kappa & 1.15d_0<d\leq 1.3d_0,\\ 0 & d>1.3d_0,\end{cases}$$

$$\mu=\begin{cases}\frac{\sqrt{3}}{4}(4-3\rho^{1/2})\kappa & 0.75d_0\leq d\leq 1.15d_0,\\ \frac{\sqrt{3}}{4}(3.9\rho^{1/2}-4)\kappa & 1.15d_0<d\leq 1.3d_0,\\ 0 & d>1.3d_0,\end{cases}$$

$$p=\begin{cases}\sqrt{3}(\rho^{1/2}-1)\kappa & 0.75d_0\leq d\leq 1.15d_0,\\ \sqrt{3}(1-1.3\rho^{1/2})\kappa & 1.15d_0<d\leq 1.3d_0,\\ 0 & d>1.3d_0.\end{cases} \tag{13}$$

where $\rho=(d_0/d)^2$ is the density relative to the stress-free state. From Eq. (13) we can see that there is a shear instability (characterized by $\mu\leq 0$) at $d=0.75d_0$. This corresponds to the transition from the triangular lattice to a square lattice.[28] At $d=1.15d_0$ both B and μ jump discontinuously to negative values. As will be seen in Sec. IV B 1, this spinodal instability is the rupture point at zero temperature. The discontinuity results from a discontinuity in ϕ'' at $d=1.15d_0$. In the other two systems the spinodal instability corresponding to rupture occurs continuously.

For the LJ monolayer (LJM), using Eq. (12) and Table I, up to the 11th neighbors, we obtain

$$\lambda = 374.732\left(\frac{\sigma}{d}\right)^{14} - 132.240\left(\frac{\sigma}{d}\right)^{8}\frac{\epsilon}{\sigma^2},$$

$$\mu = 208.183\left(\frac{\sigma}{d}\right)^{14} - 43.9324\left(\frac{\sigma}{d}\right)^{8}\frac{\epsilon}{\sigma^2},$$

$$p = 83.2729\left(\frac{\sigma}{d}\right)^{14} - 44.1538\left(\frac{\sigma}{d}\right)^{8}\frac{\epsilon}{\sigma^2}. \quad (14)$$

The only instability point in this system is the rupture spinodal instability characterized by B going negative at $d=1.2207\sigma(=1.0875d_0)$ or $p=-3.8521\epsilon/\sigma^2(=-0.1092\kappa)$.

Similarly for the 4-8 monolayer (4-8M), and also up to the 11th neighbors, we find

$$\lambda = 197.31\left(\frac{\sigma'}{d}\right)^{10} - 86.707\left(\frac{\sigma'}{d}\right)^{6}\frac{\epsilon'}{\sigma'^2},$$

$$\mu = 84.530\left(\frac{\sigma'}{d}\right)^{10} - 16.808\left(\frac{\sigma'}{d}\right)^{6}\frac{\epsilon'}{\sigma'^2},$$

$$p = 56.389\left(\frac{\sigma'}{d}\right)^{10} - 34.949\left(\frac{\sigma'}{d}\right)^{6}\frac{\epsilon'}{\sigma'^2} \quad (15)$$

In this case also the only instability point is the rupture spinodal instability at $d=1.285\sigma'(=1.080d_0)$ or $p=-3.168\epsilon'/\sigma'^2(=-0.101\kappa)$.

We expect that, at zero temperature, rupture will occur at this mechanical instability point, but that, at finite T, it will not be so. For a range of $|p|<|p_c|$, the free energy barrier can be so small that local thermal fluctuations will be enough to overcome it. We illustrate this in Sec. IV.

IV. SIMULATIONS ON THE TWO-DIMENSIONAL SOLID MEMBRANES

A. Methods

In our MD simulations, the TpN ensemble[29–31] was used for the kinetics, suplemented by the TVN ensemble[32–34] for the calculation of the elastic constants. The basic time step was $\tau_0=0.05t_0$, where $t_0=\sqrt{m/\kappa}$. A critical rupture pressure p_c is defined as the pressure for which the membrane ruptures in about 5×10^5 time steps. This definition of p_c is based on the assumption of an exponential decrease of the rupture time with increasing $|p|$, a reasonable assumption for a thermally activated process. The above assumption is verified in the simulations. Within 5% of p_c are intervals of p of rapid rupture (less than 10^4 time steps) and no observed rupture over times in excess of 3×10^6 time steps. The motivation for the use of $5\times10^5\tau_0$ as the maximum rupture time is based on the observation that by that time, the systems appeared well equilibrated.

The paths to rupture consisted in a slow increase of the tension $|p|$, in small steps $|\Delta p|$, from an initial perfect lattice configuration. For each value of $|p|$ the system was allowed to equilibrate well (at least during time $5\times10^5\tau_0$). $|\Delta p|$ was a function of the temperature, the range of interactions, and whether $|p|>|p_c|$. The higher the temperature and the longer the range of interactions, the smaller $|\Delta p|$ as $|p_c|$ itself was smaller. For instance, for the PLFM at $T=0.0005\kappa d_0^2/k_B$ and $|p|<|p_c|$, $|\Delta p|=0.001\kappa$. But for the PLFM at $T>0.006\kappa d_0^2/k_B$ and $|p|<|p_c|$, $|\Delta p|=0.0002\kappa$. For the LJM and 4-8M at $T>0.006\kappa d_0^2/k_B$ and $|p|<|p_c|$, $|\Delta p|=0.0001\kappa$, half of what was used in the PLFM. It is therefore reasonable to state that the tension rates in our systems were low.

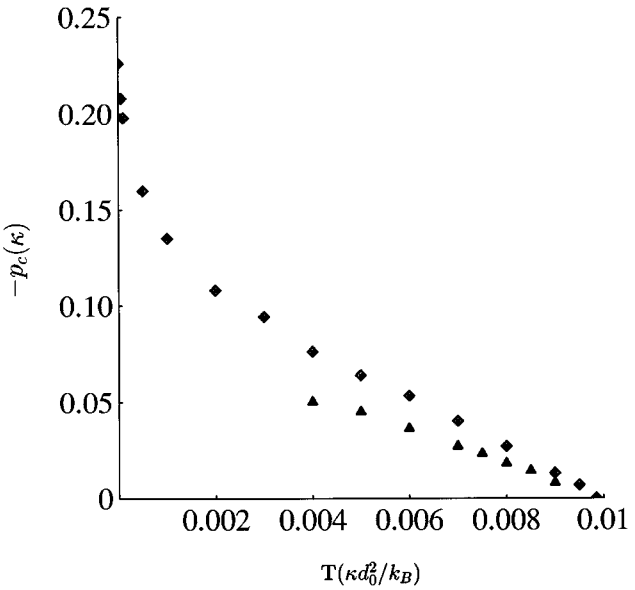

FIG. 1. The variation of $|p_c|$ vs T for the two-dimensional perfect solid PLFM (solid diamond) and PLFM with a vacancy concentration of 2.56 at. % (solid triangle).

For convenience of comparison, for our equal depth potentials, p is in units of κ and T in units of $\kappa d_0^2/k_B$. For the LJM, to convert p to ϵ/σ^2 and T to ϵ/k_B, multiply by 35.2756 and 44.4444, respectively. For the 4-8M, to convert p to ϵ'/σ'^2 and T to ϵ'/k_B, multiply by 31.4270 and 44.4444, respectively.

Most of the simulations are for rhombuses with 28 atoms on the side. We also tried samples with 51 atoms on the side to check size effects.

B. Critical quantities

1. At zero temperature

The set of Figs. 1 to 5 show the critical rupture pressure p_c and the corresponding values at rupture of the lattice constant d_c, bulk modulus B_c, and shear modulus μ_c, as a function of temperature. All these quantities tend to their mechanical instability point when $T\rightarrow0$; this is the case for all three kinds of potentials, where the values of p_c, d_c, B_c, and μ_c at $T=0$ are obtained from Eqs. (13)–(15). This supports the approach taken in Sec. III, that the rupture point at zero temperature is a mechanical instability point. More specifically, at zero temperature it is a spinodal instability point, where B goes through zero continuously in the LJM and 4-8M, and jumps to negative values in the PLFM.

No other instability was found for either the LJM or 4-8M in the analysis of the elastic constants in Sec. III. Numerical simulations on the LJM in the TpN ensemble at $T=0.0022\epsilon/k_B$ with pressures up to $p=2100\epsilon/\sigma^2$ support this prediction.

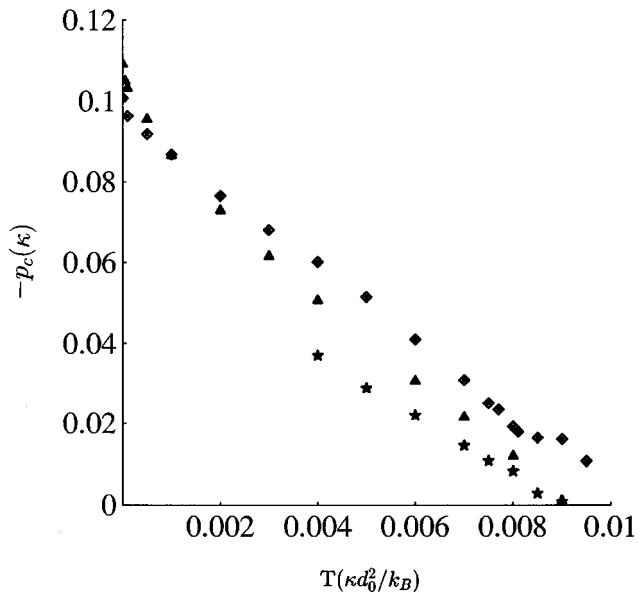

FIG. 2. The variation of $|p_c|$ vs T for the two-dimensional perfect solid LJM (solid triangle), LJM with vacancy concentration of 2.56 at. % (star), and perfect 4-8M (solid diamond).

2. At finite temperature

The first observation that can be made from Figs. 4 and 5 is that, as expected, at finite temperature, rupture occurs prior to mechanical instability, since both B and μ greater than zero at the critical pressure. Second, Figs. 1–5 show clearly that there are two temperature regimes for all three kinds of interactions. The first regime, at low temperature, is characterized by a fast nonlinear drop of $|p_c|$ from the zero-temperature instability point. The second regime at higher temperatures is characterized by an almost linear decrease of $|p_c|$ with T, with or without vacancies. These two regimes represent different rupture kinetics, as we will discuss in the next section.

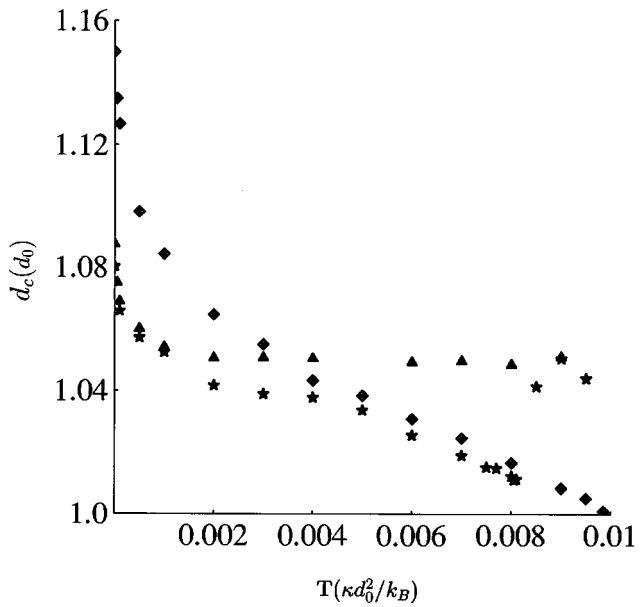

FIG. 3. The variation of d_c vs T for the two-dimensional perfect solid PLFM (solid diamond), LJM (solid triangle), and 48M (star).

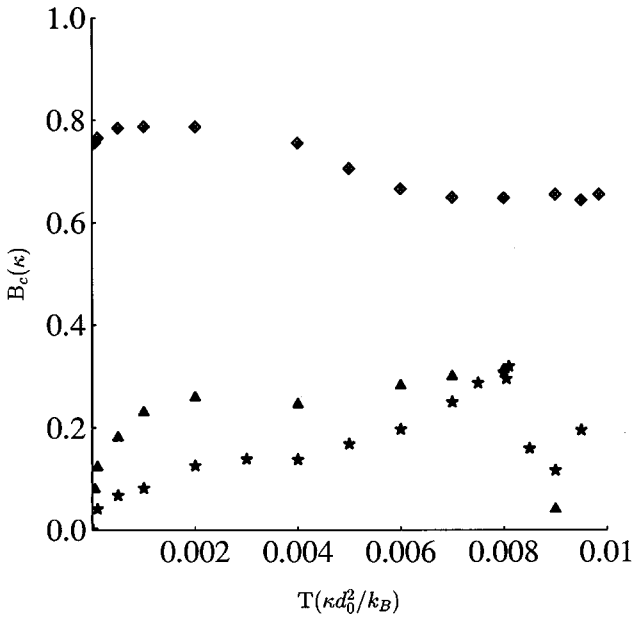

FIG. 4. The variation of B_c vs T for the two-dimensional perfect solid PLFM (solid diamond), LJM (solid triangle), and 48M (star).

Figure 5 also shows that the shorter the range of interaction the larger μ_c is. Since the Rayleigh speed, the upper limit of the velocity of crack propagation, is approximately equal to the transverse sound speed,[35,36] which itself is proportional to $\sqrt{\mu/\rho}$ (ρ is the density), we can expect that the shorter the range of the interaction, the faster the crack will propagate. This has been verified in the simulations.

We also find that the PLFM and LJM remain solid up to the point of rupture ($\mu>0$ and $B>0$ for $|p|<|p_c|$). But for $T>0.008\kappa d_0^2/k_B$, the 4-8M, with the interaction of the longest range, melts first (lattice constant increases suddenly and $\mu=0$) and then ruptures. The liquid PLFM and LJM rupture under minimal stresses. These facts limit the use of these potentials to the study of rupture in the solid phase.

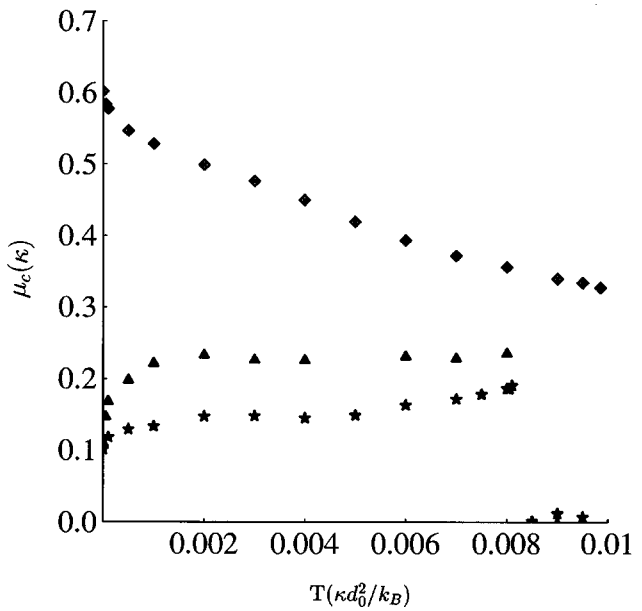

FIG. 5. The variation of μ_c vs T for the two-dimensional perfect solid PLFM (solid diamond), LJM (solid triangle), and 48M (star).

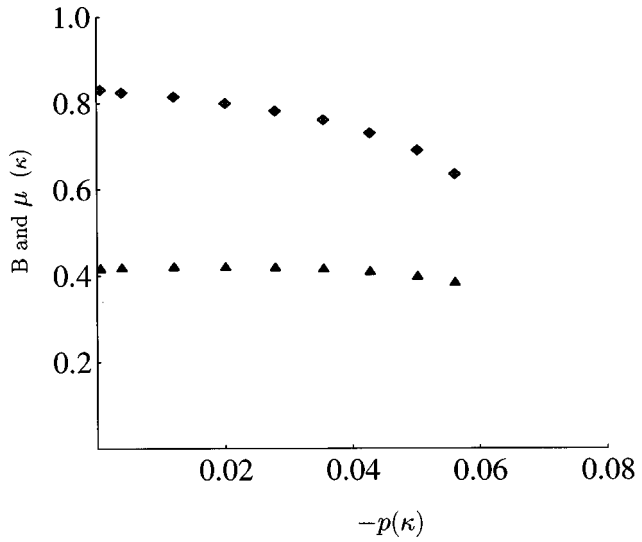

FIG. 6. The variation of B (diamond) and μ (solid triangle) vs p for two-dimensional perfect PLFM at $T=0.006\kappa d_0^2/k_B$. $p_c=0.0508\kappa$.

3. Precursor effects to rupture

At zero temperature, as follows from Eqs. (13)–(15), the mechnical instability point, which coincides with the rupture point, corresponds to an extremum in the tension $-p$. At finite temperature, the two points do not coincide. Rupture occurs before mechanical instability. However, we found precursor effects in both B and μ; an accelerated drop around p_c, especially in the PLFM and the LJM (see Figs. 6 and 7 for some typical results). This is reminiscent of the precursor effects, observed in the compressibility at melting, which have been investigated by Boyer.[37] He argued that their presence makes melting in solids exhibiting this effect less abrupt, i.e., with less of a jump in the thermodynamic functions.[17]

In our case, with relation to rupture, the precursor effects permit an easier identification of the critical rupture pressure.

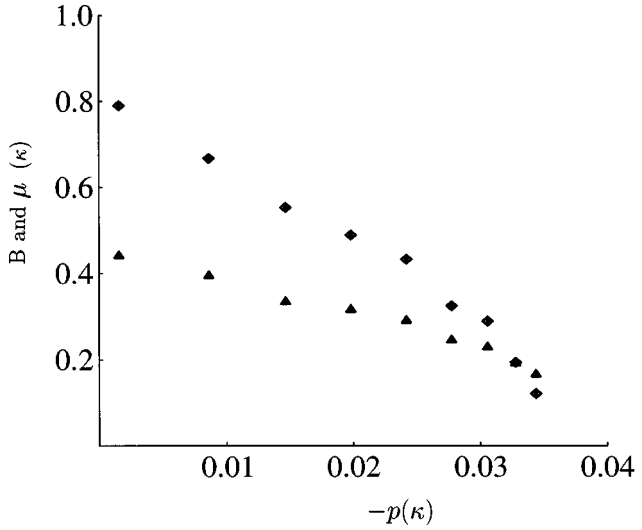

FIG. 7. The variation of B (diamond) and μ (solid triangle) vs p for two-dimensional perfect LJM at $T=0.006\kappa d_0^2/k_B$. $p_c=0.0300\kappa$.

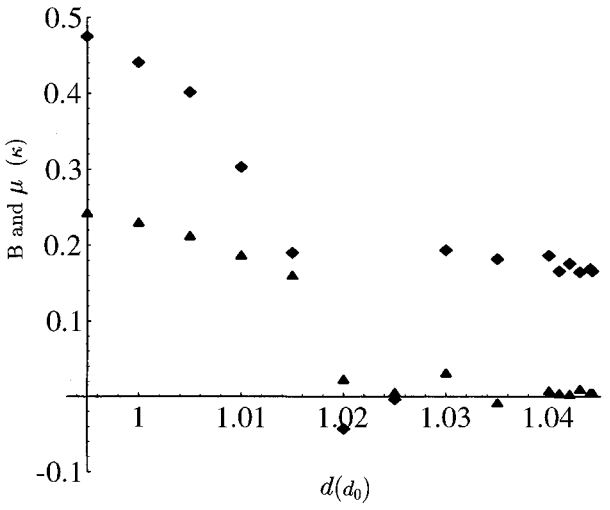

FIG. 8. The variation of B (diamond) and μ (solid triangle) vs d for two-dimensional perfect 4-8M at $T=0.0085\kappa d_0^2/k_B$. $d_c=1.041d_0$ and $p_c=0.0164\kappa$.

But, on the other hand, they make it harder to extrapolate to the mechanical instability point. This point has been found to be inaccessible by either the TpN or the TVN ensemble. We observed that, in the TVN ensemble, slightly above the rupture point (within about 10% of p_c), that the average B (often <0) and μ are highly unstable even up to $10^6\tau_0$ in simulations and also sensitive to the initial conditions (configuration and velocity). In contrast, the same quantities below the rupture point are very stable within less than $10^5\tau_0$. In the intermediate region occurs the accelerated drop in B and μ around p_c—the precursor effects shown in Figs. 6 and 7 for the PLFM and LJM, respectively. They become more pronounced with increasing temperature and range of interaction. The latter fact is illustrated by comparing the effect in the LJM with that in the PLFM which has nearest-neighbor interactions.

The TVN ensemble, which is a better ensemble as a rule to calculate elastic constants,[27] should be used to identify the rupture point. Since B drops more rapidly than μ near rupture, it is the quantity to follow. Typically, in the TVN ensemble, $10^5\tau_0$ is enough to obtain rather good results for B, μ, and p. But in the TpN ensemble, we have to run some samples to over $3\times10^6\tau_0$.

In the 4-8M, which melts before rupturing, both B and μ drop to zero at the melting point, making the identification of this transition easy (see Fig. 8). B then rises after melting. There is no evidence of precursor effects in this state.

C. Rupture kinetics

The rupture kinetics are investigated in the TpN ensemble, which allows larger fluctuations and is closer to normal experimental conditions. The observed behavior is quite different at low T than at high T.

At very low temperature, for the PLFM and LJM, rupture is mainly through the propagation of a single crack, accompanied by a homogeneous area expansion. A small crack nucleates and grows. At a certain size L, the crack begins to branch out. L is dependent on the temperature, the range of interaction, and the initial conditions of the simulation. It is typically a few lattice constants (5 to 9).

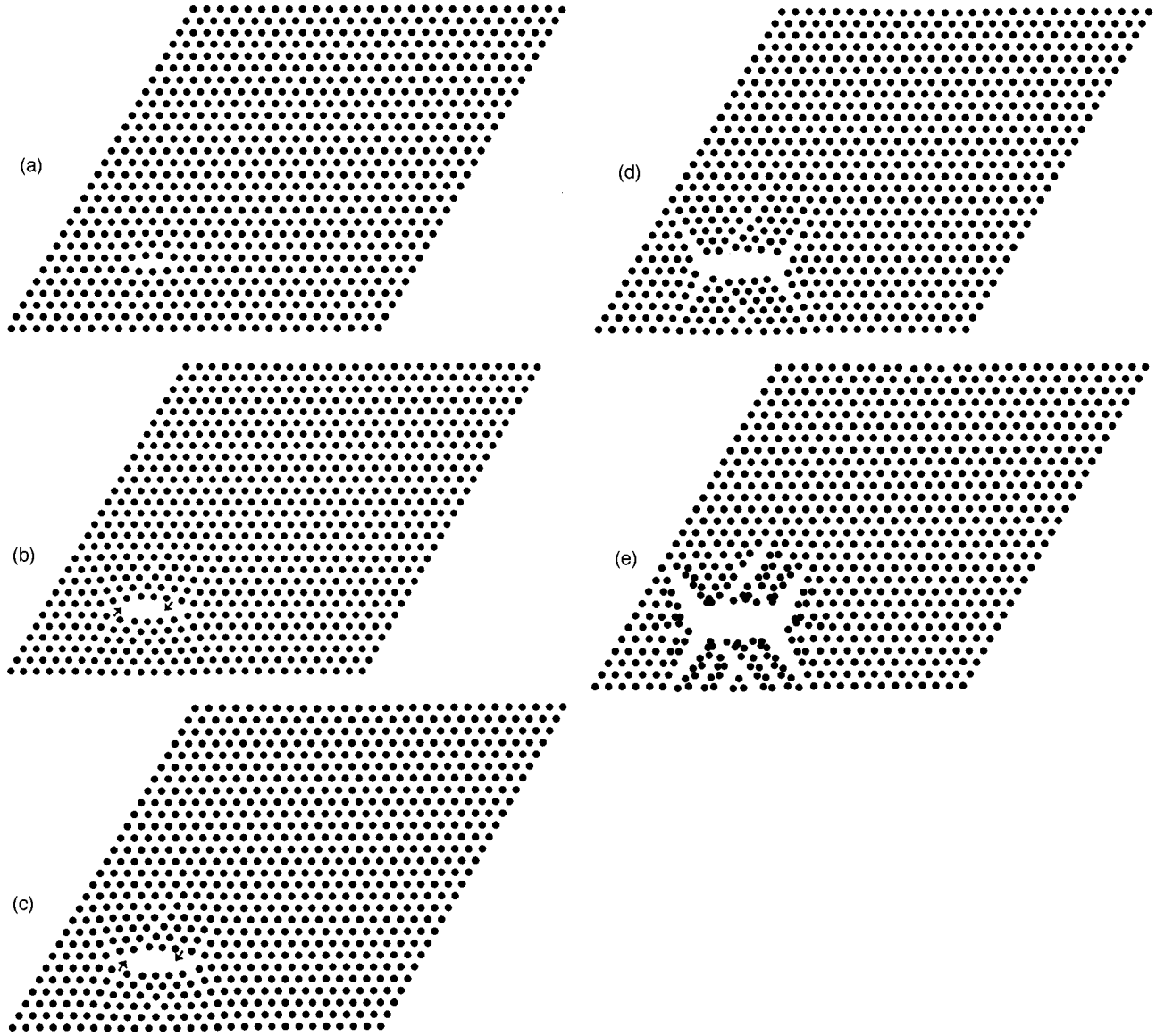

FIG. 9. Configurations of atoms at various times t for the LJM at $T=0.00005\kappa d_0^2/k_B$ and $p=-0.1055\kappa$. (a) $t=1750\tau_0$, (b) $t=1950\tau_0$, (c) $t=2000\tau_0$, (d) $t=2100\tau_0$, (e) $t=2450\tau_0$. The arrows represent the Burgers vectors of the dislocations and are placed at their core.

Under isotropic tension, the crack always propagates along ''soft'' directions, i.e., the directions with the lowest surface energy. It agrees with the conventional wisdom which would identify the lowest energy surface as the cleavage direction, but is obviously different from that observed under uniaxial tension where fracture can occur along a ''stiff'' direction, i.e., a direction of high surface energy.[36]

Crack branching has also been observed in brittle materials under uniaxial tension or with a temperature gradient, in both experimental and theoretical studies.[38–41] However, in a uniaxial tension experiment this requires large values of the strain rate or temperature gradient.[36,38,39] At small strain rate, the cracks do not seem to branch out.[36,39] In systems under isotropic tension, the situation is quite different. The stress builds up in all direction. This favors, or maybe even requires, crack branching.

Note that there are two competitive factors in rupture kinetics. One is the area expansion or the increase in the lattice constants. This is a homogeneous process. The other is the growth of the crack, which is a heterogeneous process. If the rate of area expansion is comparable with the propagation speed of the crack, the system may eventually rupture homogeneously. This happens at very low temperature. Increasing the range of interaction favors homogeneous rupture. A longer range of interaction induces a longer correlation length which favors a collective response to the strain. For the LJM, we observed that the system finally ruptures homogeneously for $T<0.002\kappa d_0^2/k_B$, but for the PLFM this occurs for $T<0.0005\kappa d_0^2/k_B$. One can expect that due to anisotropy, a system under uniaxial tension does not exhibit homogeneous rupture.[36]

Figure 9 shows a rupture sequence for a LJM at $T=0.00005\kappa d_0^2/k_B$ and $|p|=0.1055\kappa$, slightly higher than $|p_c|$ $(=0.105\kappa)$. At time $t=1750\tau_0$, a crack is nucleated, as shown in Fig. 9(a). At $t=1950\tau_0$, the size of the crack in-

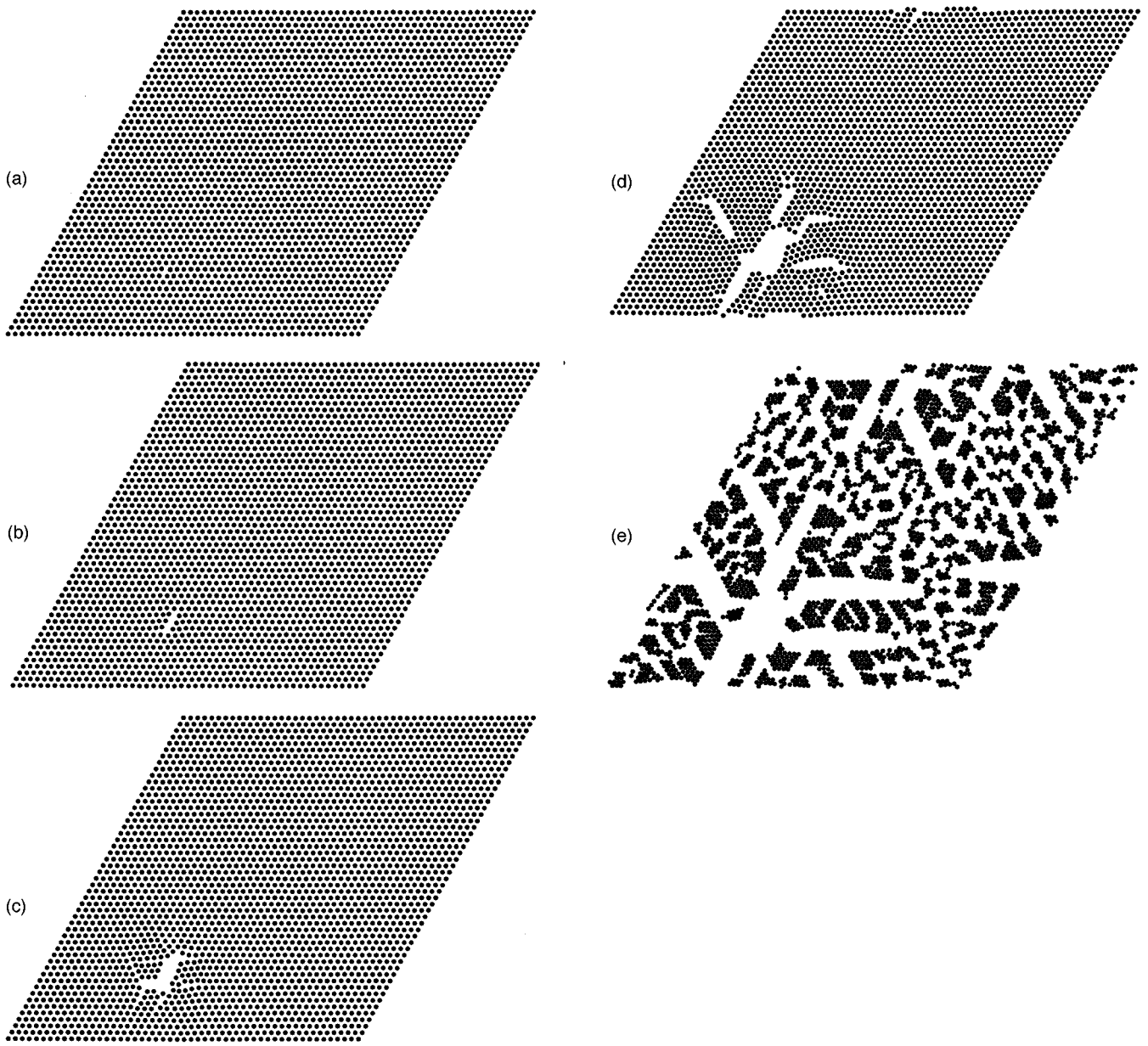

FIG. 10. Configurations of atoms at various times t for the PLFM at $T=0.0005\kappa d_0^2/k_B$ and $p=-0.168\kappa$. (a) $t=800\tau_0$, (b) $t=860\tau_0$, (c) $t=1000\tau_0$, (d) $t=1280\tau_0$, (e) $t=2200\tau_0$.

creases to about $5d$ with $d=1.088d_0$, and a dislocation dipole can be seen, as shown in Fig. 9(b). At $t=2000\tau_0$, the crack begins to branch out as shown in Fig. 9(c). At about $t=2100\tau_0$ (Fig. 9(d)), the crack stops growing and the faster area expansion completes the rupture process. At $t=2450\tau_0$, the average lattice constant $d=2.887d_0>3\sigma$, the cutoff of LJP, so the system has ruptured homogeneously [Fig. 9(e)].

Figure 10 shows a rupture sequence for a PLFM of size 51×51 at $T=0.0005\kappa d_0^2/k_B$ and $|p|=0.168\kappa$ ($|p_c|=0.160\kappa$). At $t=800\tau_0$, a crack is nucleated, as shown in Fig. 10(a). The crack then grows to a size of $L=3d$ at $t=860\tau_0$. At this size, the crack begins to branch out, as shown in Fig. 10(b). At $t=1000\tau_0$, we can see a second branching out of the original crack, as shown in Fig. 10(c). In Fig. 10(d) a third branch in the crack occurs at $t=1280\tau_0$. Finally at $t=2200\tau_0$, the system ruptures [Fig. 10(e)]; a clear case of a heterogeneous process.

As mentioned in Sec. IV B 2 crack propagation is the fastest in the shorter range systems. For instance, at low temperature, for the PLFM at $T=0.00005\kappa d_0^2/k_B$, the time duration from the crack nucleation to a crack of size $5d$ is about $130\tau_0$, but for the LJM growth to the same size requires $200\tau_0$. The thermal fluctuations reduce the crack velocity in two ways. First it favors asymmetric stresses around the tip of the crack, and hence nonrectilinear motion which reduces the forward velocity of the crack. Secondly it weakens the solid, with the ensuing effect on crack velocity.

The high-temperature dynamics are different. At high temperature, gliding dislocation dipoles are created first, which then develop into holes. Ingrown vacancies limit the role of dislocations and can lead to direct cavitation. Irre-

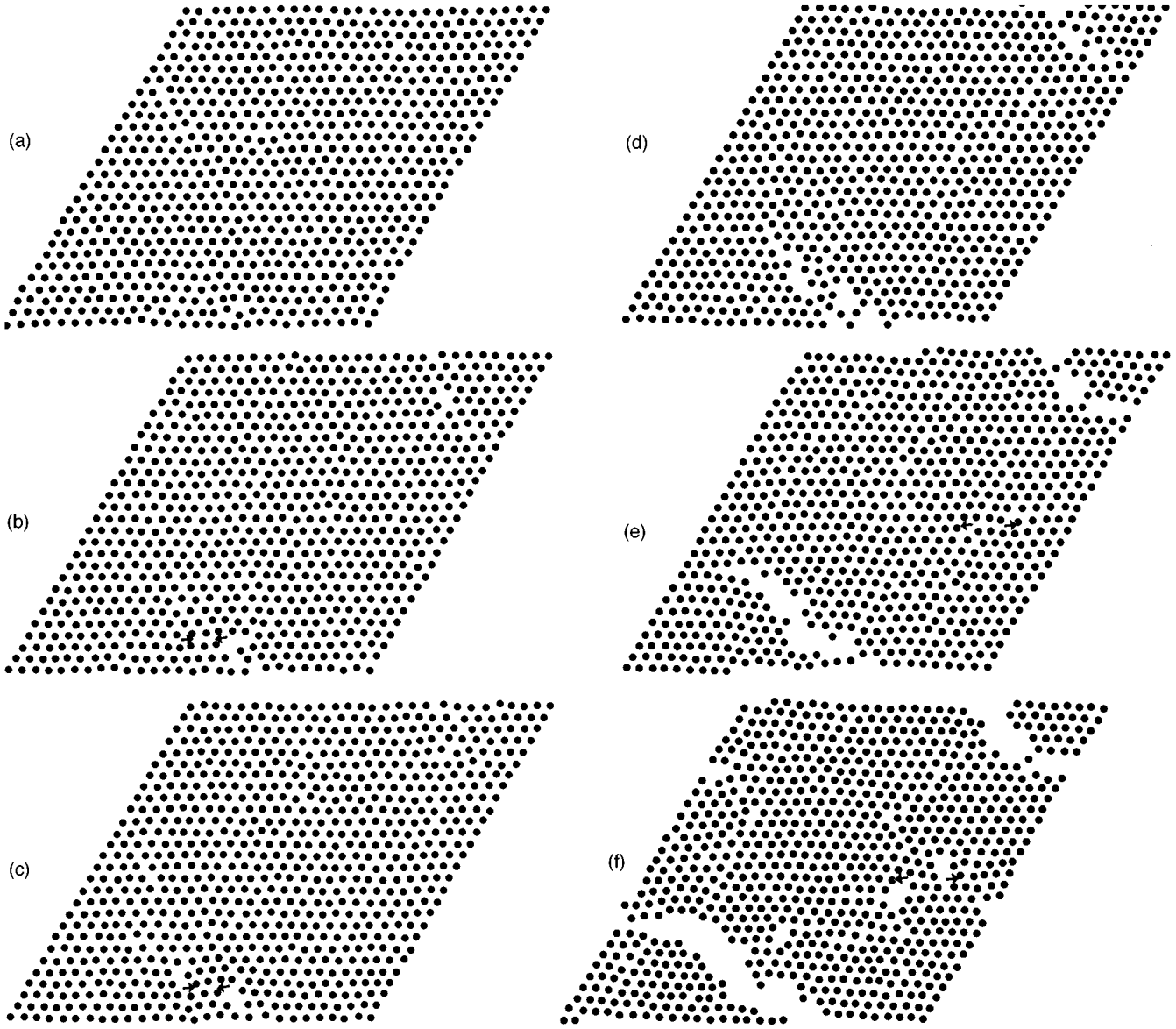

FIG. 11. Configurations of atoms at various times t for the PLFM at $T=0.006\kappa d_0^2/k_B$ and $p=-0.0550\kappa$. (a) $t=28100\tau_0$, (b) $t=28650\tau_0$, (c) $t=28750\tau_0$, (d) $t=29200\tau_0$, (e) $t=29400\tau_0$, (f) $t=29600\tau_0$.

spective of the presence of the ingrown vacancies, the system becomes porous before rupture, and rupture is mainly via the merger of holes. Furthermore, pores become more prevalent as the range of interparticle interactions increases. The material is more ductile.

The temperature T_1 separating these two regimes is dependent on the range of interaction. The shorter the range of interaction, the higher T_1. In other words, the shorter the range of the interaction, the larger the temperature range for the fast nonlinear drop of $|p_c|$. This is because the short-range interaction favors the formation of a single large crack. In systems with long-range interaction the formation of dislocation dipoles is favored, as was discussed in Ref. 27. For the PLFM, $T_1\approx 0.0035\kappa d_0^2/k_B$. For the LJM, $T_1\approx 0.0025\kappa d_0^2/k_B$. But for the 4-8M, $T_1<0.000025\kappa d_0^2/k_B$. And below $0.00002\kappa d_0^2/k_B$, we observe homogeneous rupture. No crack was ever seen in this last system.

Figure 11 shows a rupture sequence for a PLFM at $T=0.006\kappa d_0^2/k_B$, higher than T_1, and $|p|=0.0550\kappa$, slightly higher than $|p_c|(=0.0534\kappa)$. At $t=28100\tau_0$, some vacancies are nuclueated, as shown in Fig. 11(a). At $t=28650\tau_0$, a dislocation dipole is created [Fig. 11(b)]. The dislocation dipole then develops into small pores [Fig. 11(c)]. Figures 11(d) and 11(e) show clearly the merger of these pores. As we can see from Fig. 11(f), at $t=29600\tau_0$, more holes and dislocations appear just before rupture.

The kinetics can explain why the mechanical stability criteria fail to predict the rupture point at finite temperature. The propagation of a single crack or the merger of holes is a heterogeneous process, but the derivation of the mechanical stability criteria assumes homogeneous deformation.[21,22]

V. EFFECT OF OUT-OF-PLANE FLUCTUATIONS: A ONE-DIMENSIONAL CLOSED MEMBRANE

In Secs. III and IV, we have discussed in detail the rupture kinetics of a flat membrane, which is constrained within

a two-dimensional space, and hence does not allow transverse fluctuations. For a real membrane there is, however, normally the third degree of freedom and transverse fluctuations will be present. To assess their effect on the rupture kinetics we consider a simple model of self-assembled membranes, which we study here in one dimension, by forming closed molecular chains. This 2D vesicle is pressurized with an ideal gas. We find two very distinct regimes of rupture behavior. At low T rupture can be explained by the average force on the membrane approaching close to the critical bond strength in the membrane. But at high T, it seems totally fluctuation driven, with the critical gas pressure bearing little connection with the average bond strength.

A. The self-assembling molecules

In the 1D closed chains or 2D vesicles, the particles are assumed to have a director **n**, which can also be considered as a main axis of symmetry. They interact through the pair potential

$$\phi(\mathbf{r_1},\mathbf{r_2})=4\epsilon\left\{\left(\frac{\sigma}{r_{12}}\right)^N-\left(\frac{\sigma}{r_{12}}\right)^M[1+\gamma f(\mathbf{r_1},\mathbf{r_2})]\right\}, \quad (16)$$

with

$$f(\mathbf{r_1},\mathbf{r_2})=\mathbf{n_1}\cdot\mathbf{n_2}-[(\mathbf{n_1}+\mathbf{n_2})\cdot(\mathbf{r_{12}})]^2. \quad (17)$$

We chose $M=6,N=12$ (Lennard–Jones-like potential or LJP) and $M=4,N=8$ (4-8 potential or 4-8P) to probe the effects of the range of the interaction. The f term in the potential introduces an orientation interaction, and γ can be used as a measure of that interaction. $\gamma=0$ gives the usual $M-N$ potential and the system tends to form a bulk even with the inclusion of a pressurizing gas. In our simulations, we chose $\gamma=0.9$, since for this value the particles can self-assemble into long chains at moderate temperatures. The interaction favors a parallel orientation of the directors (i.e., $\mathbf{n_1}\cdot\mathbf{n_2}=1$). The cutoff was chosen to be $r_c=3.0\sigma$ for LJP and $r_c=3.0^{1.5}\sigma$ for 4-8P. The unit of time in the simulations is $t_0=\sqrt{m\sigma^2/\epsilon}$.

To deal with the changes in direction of the main axis **n**, a rotational inertia I was introduced. $I=1/2m\sigma^2$ was chosen for convenience, where m is the mass of the particles.

Pressure inside the vesicle is produced with a gas of particles, of mass equal to the particles forming the chain. These particles interact with the particles of the vesicles with a $1/r^{12}$ law, but not with each other. The pressurizing gas is essentially an ideal gas. Changing the mass of the gas particles could modify the kinetics.

B. The simulations

The isothermal-isochore TVN ensemble[32–34] was used with the damped force method[34] to keep the temperature constant. The basic time step in most of our simulations is $\tau_0=0.005t_0$, where $t_0=\sqrt{m\sigma^2/\epsilon}$. We also tried for some samples $\tau_0=0.0025t_0$ but there was no significant change. Following the same argument as in Sec. IV, a critical rupture pressure p_c could be easily determined as the pressure separating intervals of p of rapid rupture and no observed rupture over 2×10^6 time steps. The intermediate region is about 2% of p_c, a little smaller than in 2D, which is expected for reasons of dimensionality. The initial configuration was a closed circular chain.

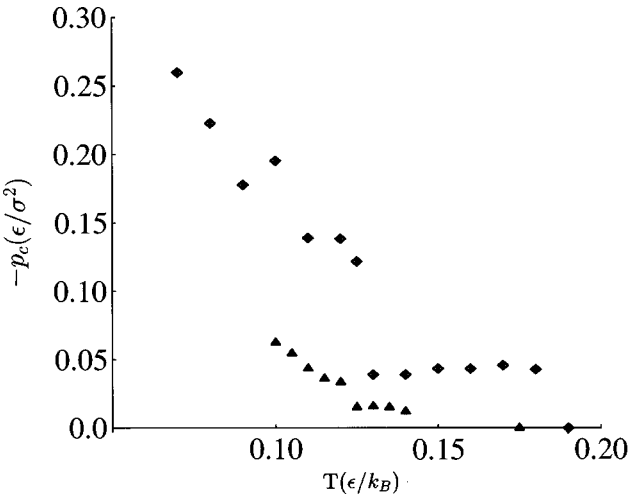

FIG. 12. The variation of $|p_c|$ vs T for a one-dimensional closed LJM of 100 particles (solid diamond) and 150 particles (solid triangle).

Since the pressurizing gas is essentially an ideal gas, we used $|p|=N_{\rm gas}k_BT/A$ to calculate the pressure, where A is the area enclosed by the chain, and $N_{\rm gas}$ the number of particles in the pressurizing gas. The area was calculated by two methods, one is $A=\pi R^2$ with $R=Nd/2\pi$. N is the number of particles in the vesicle, d the average distance between the nearest neighbors. The justification of this expression is that in our simulations the vesicle is always nearly circular up to rupture. The other method is to use $A=1/2\Sigma_i^N(y_i+y_{i+1})(x_i-x_{i+1})$ with $x_{N+1}=x_1$ and $y_{N+1}=y_1$. The results of both methods were consistent.

C. Results

From Figs. 12–14, we can see that there are also two regimes, separated by a special temperature named T_2, in the variation of p_c vs T, and d_c, the corresponding critical lattice constant, vs T. There is a fast decrease of $|p_c|$ and d_c

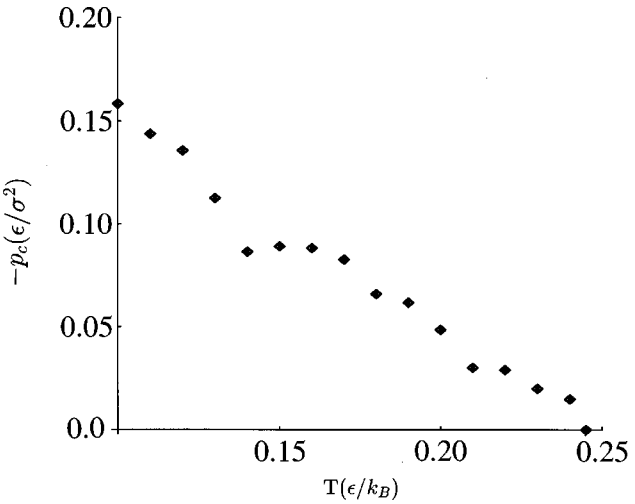

FIG. 13. The variation of $|p_c|$ vs T for a one-dimensional closed 4-8M of 100 particles.

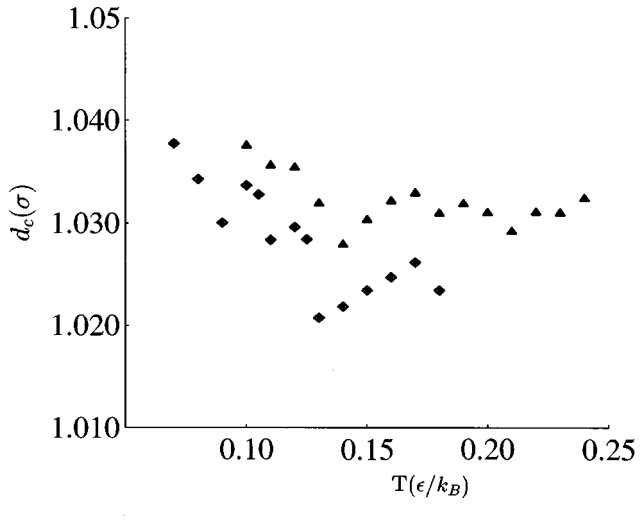

FIG. 14. The variation of d_c vs T for a one-dimensional closed LJM with 100 particles (solid diamond) and 4-8M with 100 particles (solid triangle).

below T_2 for both LJP and 4-8P interactions. This is the expected behavior for a thermally activated process. At T_2, a sudden drop of $|p_c|$ and d_c occur for the LJP. There is no such drop in the 4-8P system. The longer range force tends to behave more smoothly. In the shorter range LJP system, p_c is nearly constant over a significant temperature interval.

T_2 is dependent on both the interaction and the size of the system. $T_2 \approx 0.125\epsilon/k_B$ with the LJP and 100 particles, $T_2 \approx 0.120\epsilon/k_B$ with the LJP and 150 particles, and $T_2 \approx 0.14\epsilon/k_B$ with the 4-8P and 100 particles.

As in the 2D case discussed in Sec. IV, one can assume that in these two regimes the rupture kinetics are different. But contrary to the 2D case, it is difficult to determine directly what causes the rupture. To gain some insight, we monitored the relationship between the critical force and the pressure at rupture in the 100 particle LJP vesicle.

At zero T, assuming that the system is a perfect circle, the relationship between the pressure and the force (F) on a particle from particles on each side is given by

$$F = 2pR, \tag{18}$$

where R is the radius of circle. It is to be expected that strong thermal fluctuations, dominantly transverse, will lead to violation of this relation. For a more detailed comparison, we also calculated $\mathcal{F} = \Phi'(d) + \Phi'(2d)$, where

$$\Phi(r) = 4\epsilon\left\{\left(\frac{\sigma}{r}\right)^N - (1+\gamma)\left(\frac{\sigma}{r}\right)^M\right\}.$$

$\mathcal{F}$ is another approximation for the force since the orientation term f in the interparticle interaction [see Eq. (17)] is always ≈ 1 in simulations. Table II, gives the values of these quantities at rupture.

From Table II, we can see that at high T, $2p_cR$ is significantly smaller than $\langle F_c \rangle$ or $\Phi'(d_c) + \Phi'(2d_c)$. But, at low T, $\langle F_c \rangle \approx \Phi'(d_c) + \Phi'(2d_c)$, and comparable to $2p_cR$. This suggests that, at about $T = 0.12$, thermal fluctuations suddenly become large enough to drive the rupture kinetics.

TABLE II. Critical quantities in 1D for system with LJP and 100 particles.

T	d_c	$2p_cR = p_cNd/\pi$	$\langle F_c \rangle$	$\Phi'(d_c) + \Phi'(2d_c)$	p_c
0.15	1.0238	1.462	5.218	3.5623	0.0449
0.14	1.0220	1.311	5.055	3.2803	0.0403
0.11	1.0283	4.548	4.750	4.4086	0.1390
0.10	1.0330	6.280	4.910	5.1368	0.1910
0.09	1.0300	5.852	4.585	4.6770	0.1785

In our simulations, the vesicle is always nearly circular up to rupture. Shape fluctuations do, however, become noticeable in the longer-range system.

Finally, we should point out that the units in this section are different from those in Sec. IV A. Converting them into the same units using the remarks in Sec. IV, we find that $|p_c|$ is much smaller than in the 2D flat membranes. However, it does not necessarily mean that the out-of-plane fluctuations are dominant. The energies of fluctuations in a 1D system scale inversely with system size, (wave vector)^2 times length L, or $(2\pi/L)^2 L \propto 1/L$. So we expected and found significant finite-size effects. We are not able for this reason to determine whether the transverse fluctuation driven regime occurs before or after the in-plane mechanism. This will be the subject of future work.

VI. SUMMARY AND DISCUSSION

We have investigated the rupture kinetics of monolayers subjected to isotropic stress, in three central-force systems with the range of the interparticle interaction going from nearest neighbor to about five lattice spacings. Here is a summary of our findings on the 2D model with in-plane kinetics.

At $T = 0$ K, rupture is by a homogeneous process, and critical stress is as predicted by stability criteria. As the temperature is raised, there is a rapid drop in the critical stress p_c. Rupture becomes a heterogeneous process and occurs below the stress values predicted by stability criteria which assume homogeneous deformation. Precursor effects in the elastic constants, in particular the bulk modulus, facilitate the identification of the rupture point. At low T, the regime of the rapid drop in p_c, the kinetics is by nucleation of a single crack, which branches out and grows till through a combination of area expansion and crack growth the monolayer fails.

At temperatures higher than some critical T_1, the rate of decrease of the critical stress slows down. Gliding dislocation dipoles are nucleated, suggesting a ductile behavior. These grow with the addition of vacancies. The holes grow and merge till failure. Ingrown vacancies reduce the influence of dislocations and can lead to direct cavitation.

Crack propagation is faster in the system with short-range force. It is prevalent in systems with nearest-neighbor interaction. The opposite is true for the longest-range force system (4-8P, cutoff at 5 σ), where a crack propagation regime is hard to identify.

The temperature T_1 separating these two regimes is dependent on the range of interaction and the shorter the range of interaction, the higher this temperature. We have also presented simple expressions for stress, bulk modulus B and shear modulus μ for systems with PLFP, LJP, and 4-8P, at

zero temperature and under isotropic tension.

Although this work focuses on the behavior of two-dimensional systems, it also throws some light on the fracture kinetics of bulk materials. Our results support the conclusion that the cleavage direction under isotropic stress is different from that under anisotropic stress. We have also shown that the crack velocity decreases with an increase in the range of interaction. This can account for the fact that the crack velocity of the modified LJP system (MLJ), used in Ref. 36, is faster than in the original LJP system. The MLJ is a nearest-neighbor interaction but the LJP has a range of several atomic sites. We will venture a comment about the method of prenotching of a single crack in materials, which is often used in studies of the fracture dynamics and the brittle-to-ductile transition. These experiments may give different rupture kinetics than if isotropic stress were applied to the system, in particular for ductile materials. With isotropic stress, cracks are more likely to branch out along the equivalent low energy surfaces. Anisotropic stress with prenotching may preempt the formation of holes in ductile materials, the favored mechanism under isotropic stress in our 2D computer simulations.

The two regimes of rupture kinetics reported seem related to the brittle-to-ductile transition. This transition is accompanied by a large increase in the dislocation density.[42] The temperature T_1 separating the two regimes, would then be the brittle-to-ductile transition temperature. This also suggests that the system with the shorter range of interaction is more brittle since T_1 is higher.

There is a parallel between the observed rupture behavior and the vacancy annealing kinetics studied in earlier papers.[20,27,43] In simulations of annealing behavior the PLFP system formed slowly cavities of varying size, the LJP system had a low temperature and pressure phase, with a similar behavior, and a higher pressure and temperature phase with a rapid dislocation mediated annealing (DMA) kinetics. The 4-8P system, with the longest-range potential, exhibited only the DMA kinetics. The presence of dislocations again indicates ductile behavior. In brittle materials, annealing could only rely on the slow diffusion of vacancies and their mutual attraction.

Biological membranes tend to be in liquidlike phases. The relevance of this work to biological systems is in showing how the role of vacancies increases as the material softens and becomes more ductile. Dislocations are generated in pairs as dipoles, which are in fact condensed lines of vacancies.[44] The ease of nucleation of dislocations appears related to the nucleation rate of vacancy clusters, or pores. There is a connection between the two. The nucleation of vacancies in a brittle material would seem much more difficult.

The 1D model system, that we studied, shows that transverse fluctuations can also drive the rupture kinetics. Whether, in a 3D vesicle, they can preempt the mechanisms discussed above is still an open issue.

ACKNOWLEDGMENTS

This work was supported by the Natural Sciences and Engineering Research Council of Canada. Useful discussions with Michael Wortis are gratefully acknowledged.

*Author to whom correspondence should be addressed. Electronic address: joos@physics.uottawa.ca

[1] W. T. Coakley and J. O. T. Deeley, Biochim. Biophys. Acta **602**, 355 (1980).
[2] D. Gallez and W. T. Coakley, Prog. Biophys. Mol. Biol. **48** (1986).
[3] S. Ohki, *Molecular Mechanisms of Membrane Fusion* (Plenum, New York, 1988).
[4] L. Song, Q. F. Ahkong, D. Georgescauld, and J. A. Lucy, Biochim. Biophys. Acta. **1065**, 541 (1991).
[5] G. V. Gass and L. V. Chernomordik, Biochim. Biophys. Acta **1023**, 1 (1990).
[6] T. Y. Tsong, Biophys. J. **60**, 297 (1991).
[7] D. Gallez, N. M. Costa Pinto, and P. M. Bisch, J. Colloid Interface Sci. **160**, 141 (1993).
[8] M. J. Grimson, J. Phys. Condens. Matter. **5**, 4749 (1993).
[9] R. R. Netz and M. Schick, Phys. Rev. E **53**, 3875 (1996).
[10] J. C. Shillcock and D. H. Boal, Biophys. J. **71**, 317 (1996).
[11] A. J. C. Ladd and W. G. Hoover, Phys. Rev. B **26**, 5469 (1982).
[12] W. G. Hoover, N. E. Hoover, and W. C. Moss, J. Appl. Phys. **50**, 829 (1979).
[13] W. G. Hoover, W. T. Ashurst, and R. J. Olness, J. Chem. Phys. **60**, 4043 (1974).
[14] W. G. Hoover, A. J. C. Ladd, and N. E. Hoover, in *Interatomic Potentials and Crystalline Defects*, edited by J. K. Lee (Metallurgical Society, Warrendale, PA, 1981).
[15] F. F. Abraham, Adv. Phys. **35**, 1 (1986).
[16] K. Strandburg, Rev. Mod. Phys. **60**, 161 (1988).
[17] B. Joós, in *Dislocations in Solids*, edited by F. R. N. Nabarro and M. S. Duesbery (Elsevier, Amsterdam, 1996), Vol. 10, p. 505.
[18] J. A. Combs, Phys. Rev. Lett. **61**, 714 (1988); Phys. Rev. B **38**, 6751 (1988).
[19] W. G. Hoover, A. J. de Groot, and C. G. Hoover, Comput. Phys. **6**, 155 (1992).
[20] B. Joós and M. S. Duesbery, Phys. Rev. Lett. **70**, 2754 (1993).
[21] J. Wang, J. Li, S. Yip, S. Phillpot, and D. Wolf, Phys. Rev. B **52**, 12 627 (1995).
[22] Z. Zhou and B. Joós, Phys. Rev. B **54**, 3841 (1996).
[23] R. N. Thurston, in *Physical Acoustics*, edited by W. P. Mason (Academic, New York, 1964), Vol. I, Pt. A.
[24] T. H. K. Barron and M. L. Klein, Proc. Phys. Soc. London **85**, 523 (1965).
[25] D. C. Wallace, *Thermodynamics of Crystals* (Wiley, New York, 1972).
[26] S. Nosé and M. L. Klein, Mol. Phys. **50**, 1055 (1983).
[27] B. Joós, Z. Zhou, and M. S. Duesbery, Phys. Rev. B **50**, 8763 (1994); Z. Zhou, Ph.D. thesis, University of Ottawa, 1996).
[28] A. J. C. Ladd and W. G. Hoover, J. Chem. Phys. **74**, 1337 (1982).
[29] D. Brown and J. H. R. Clarke, Mol. Phys. **51**, 1243 (1984).
[30] H. C. Andersen, Chem. Phys. **72**, 2384 (1980).
[31] D. J. Evans and G. P. Morriss, Chem. Phys. **77**, 63 (1983); Phys. Lett. **98A**, 433 (1983).
[32] L. V. Woodcock, Chem. Phys. Lett. **10**, 257 (1970).
[33] Y. Hiwatari, E. Stoll, and T. Schneider, J. Chem. Phys. **68**, 3401 (1978).
[34] W. Hoover, Physica A **118**, 111 (1983).

[35] W. G. Hoover, *Computational Statistical Mechanics* (Elsevier, Amsterdam, 1991).
[36] F. F. Abraham, D. Brodbeck, R. A. Rafey, and W. E. Rudge, Phys. Rev. Lett. **73**, 272 (1994); F. F. Abraham, *ibid.* **77**, 869 (1996).
[37] L. L. Boyer, Phase Transit. **5**, 1 (1985).
[38] A. Yuse and M. Sano, Nature (London) **362**, 329 (1993); M. Marder, *ibid.* **362**, 295 (1993).
[39] M. Marder and X. Liu, Phys. Rev. Lett. **71**, 2417 (1993).
[40] E. Sharon, S. P. Gross, and J. Fineberg, Phys. Rev. Lett. **74**, 5096 (1995); **76**, 2117 (1996).
[41] P. Heino and K. Kaski, Phys. Rev. B **54**, 6150 (1996).
[42] C. St. John, Philos. Mag. **32**, 1193 (1975); M. Khantha, D. P. Pope, and V. Vitek, Phys. Rev. Lett. **73**, 684 (1994).
[43] Z. Zhou and B. Joós, Surf. Sci. **323**, 311 (1995).
[44] B. Joós, Q. Ren, and M. S. Duesbery, Surf. Sci. **302**, 385 (1994).